Impurity Effects on Bound States in the Vortex Core of Topological S-wave Superconductor

Yusuke Masaki¹* and Yusuke Kato²

¹Department of Physics, The University of Tokyo, Tokyo 113-0033, Japan ²Department of Basic Science, The University of Tokyo, Tokyo 153-8902, Japan

We study the impurity effects on the Caroli-de Gennes-Matricon (CdGM) states, particularly on the level spacings in a vortex core in topological s-wave superconductor (SC) by two means, numerically and analytically. The topological s-wave SC belongs to the same class as a chiral p-wave SC and thus there are two inequivalent vortices in terms of any symmetry operation. We take into account this inequivalence and numerically calculate the scattering rates based on an improved version of Kopnin-Kravtsov (iKK) scheme, which enables us to treat the discrete levels in the presence of white-noise disorder. We also construct the Andreev equation for the topological s-wave SC and obtain the Andreev bound states analytically. We use a correspondence between the wave functions for the Bogoliubov-de Gennes equation and the Andreev equation in the iKK scheme and deduce the formula of scattering rates described by the wave function for the Andreev equation. With this formula, we discuss the origin of impurity scattering rates for CdGM states of topological s-wave SC and the dependence on the types of vortices related to the inequivalence.

1. Introduction

An implementation of topological quantum computation (TQC) with low decoherence is promising application of topological superconductors (TSC).^{1,2)} In addition to this applicational fascination, recent intensive researches of TSC are motivated by fundamental interest in the appearance of Majorana fermion in the condensed matter physics.^{3,4)} The Majorana fermion exists as a topologically protected zero energy bound state near the edge or around the topological defects in TSC and this zero energy state obeys a non-Abelian statistics. The implementation of TOC is realized via the braiding operation among the degenerated Majorana zero energy states. 1,5) It is necessary to perform the braiding operation adiabatically in order to avoid non-adiabatic transitions of zero energy states. The typical operation time is required to be longer than the time given by \hbar divided by the level spacing between the Majorana state and the first excited state (we call this condition "adiabatic condition"). It is, thus, important that the level spacing, i.e. the energy of the first excited state is stable against disorder as well as the zero energy state also in terms of the signal strength of measurements.^{6,7)} In this work, we focus on the Majorana state in a vortex core and investigate the impurity effects on the bound states in a vortex core called Caroli-de Gennes-Matricon (CdGM) states.⁸⁾

A chiral p-wave SC^{1,9–11)} is a typical two dimensional TSC which belongs to the time-reversal broken Bogoliubov-de Gennes (BdG) class called "class D". This class is one of ten symmetry classes obtained by Altland and Zirnbauer based on the random matrix theory, ¹²⁾ and all possible TSCs are classified into these classes by Schnyder *et al.* ^{13,14)} if we do not take into account the crystal symmetry. TSC in class D has two inequivalent single vortices in terms of symmetry operations:

the inequivalence is characterized by the relative sign of chirality and vorticity. There is a remarkable difference between two inequivalent vortices, according to an earlier work about impurity effects on low energy states localized in a vortex core in chiral p-wave SC by means of quasiclassical theory. 15,16) The scattering rates of the localized states are almost same as those in the normal states when the relative sign is positive. On the other hand, the scattering rates are vanishingly small when the sign is negative. This is a consequence of coherence effects and rotational symmetry. However Sr₂RuO₄, a candidate for a chiral p-wave SC, has a point group symmetry C_4 in the crystal structure¹⁷⁾ and we could not expect to observe the effect of rotational symmetry. Other possible candidates for class D TSC are, for example, v = 5/2 fractional quantum Hall state^{11,18)} and some engineered TSC such as the surface of topological insulator with s-wave pair potential¹⁹⁾ and the semiconductor-heterostructure with an s-wave SC and a ferromagnet.²⁰⁾ The latter engineered TSC, which is described as the two dimensional electron gas (2DEG) with Rashba type spin orbit coupling (SOC), Zeeman coupling and s-wave pair potential and we call topological s-wave SC, has the rotational symmetry derived from the 2DEG realized in the semiconductor heterostructure. We expect that the impurity effects dependent on the symmetry will be observed more clearly in this system.

There are several ways to treat the impurity effects on localized states in a vortex core. The impurity strength Γ_n should be small such that the low energy spectra are discrete, since our motivation is to discuss the level spacing in the presence of impurities. In this case, we can not use the quasiclassical theory, in which the spectra are treated as continuous. Moreover, the Born parameter should be vanishingly small. In this case there are many but weak scatterers

1

^{*}masaki@vortex.c.u-tokyo.ac.jp

and (self-consistent) Born approximation is valid. In a typical unconventional superconductor, the density of states are formed around the Fermi energy if the Born parameter is not small.²³⁾ Even in an s-wave SC, the impurities, the Born parameter of which is not small, lead to the level mixing and the Landau-Zener transition.^{24–26)} Considering the above discussions, we can calculate the impurity effects by means of Kopnin-Kravtsov scheme,²⁷⁾ where they use Green's function for CdGM mode with impurity self energy (self-consistent Born approximation (SCBA)) keeping the levels discrete. We have improved their scheme in terms of the coherence factor and applicability to various kinds of SC in addition to an s-wave SC and call this scheme improved Kopnin-Kravtsov (iKK) scheme.²⁸⁾

The aim of this paper is to understand the impurity effects on the level spacing related to the adiabatic condition, and the physical picture of these impurity effects. In order to attack these issues, at first we numerically calculated the scattering rates of the vortex core states based on the iKK scheme and evaluate the property of minigap for topological s-wave SC in the presence of impurities, in terms of two inequivalent vortices. In this case, the sign of chirality related to the chiral edge mode is determined by the sign of Zeeman coupling.²⁹⁾ We find that the obtained numerical results are more complicated than those for chiral p-wave SC, which have been understood only by considering the type of vortex. We then make use of Andreev approximation^{30–32)} in order to understand the physical picture of these results and the origin of scattering rates. The physical picture can be successfully understood by considering the combinations of two types of vortices for chiral p-wave SC. Although the Andreev approximation is a kind of quasiclassical theory, we can use it to obtain the physical picture after numerical calculation based on the quantum theory.

We take $\hbar = 1$ throughout this paper.

2. Model and Method

We consider the two-dimensional superconducting system described by the following Hamiltonian:¹⁹⁾

$$H = \int d\mathbf{r} \underline{\psi}^{\dagger}(\mathbf{r}) \hat{H}_{0} \underline{\psi}(\mathbf{r}) + \int d\mathbf{r} \left[\Delta(\mathbf{r}) \psi_{\uparrow}^{\dagger}(\mathbf{r}) \psi_{\downarrow}^{\dagger}(\mathbf{r}) + \text{h.c.} \right], (1)$$

$$\hat{H}_{0} = \left(\frac{\mathbf{p}^{2}}{2m} - \mu + \alpha(\mathbf{p} \times \hat{\boldsymbol{\sigma}})_{z} + V_{z} \hat{\boldsymbol{\sigma}}_{z} \right), \ \underline{\psi}^{\dagger}(\mathbf{r}) = (\psi_{\uparrow}^{\dagger}(\mathbf{r}), \psi_{\downarrow}^{\dagger}(\mathbf{r})), \tag{2}$$

where μ , α and V_z denote chemical potential, strength of Rashba SOC and Zeeman coupling. $\hat{\sigma}_{x,y,z}$ are 2 by 2 Pauli matrices and the symbol $\vec{}$ denotes a two-component vector. The second term in the right-hand side of Eq. (1) describes s-wave superconductivity. We consider an isolated vortex in the center of two dimensional disc with radius R and set as $\Delta(r) = \Delta(r)e^{i\kappa\theta}$, where κ is the vorticity and takes the value ± 1 . We also assume that $\Delta(r)$ approaches to a constant value $\Delta_0(>0)$ far from the vortex core. When $V_z^2 > \mu^2 + \Delta_0^2$ is satisfied, the system is in the topological phase and Majo-

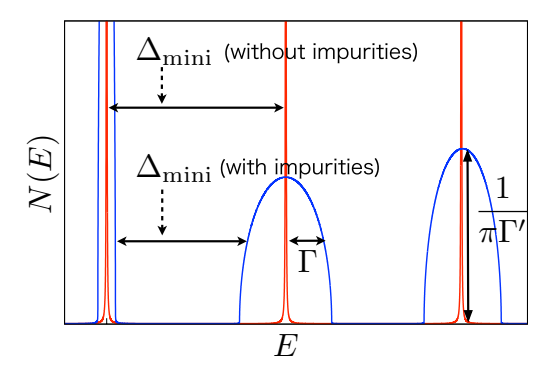


Fig. 1. (Color Online) The relations between spectra and impurity scattering rates and minigap are shown schematically.

rana zero energy states appear in the vortex core and near the edge. From the above Hamiltonian, we can obtain the following BdG equation:

$$\check{H}_{BdG}(\mathbf{r})\vec{u}_K(\mathbf{r}) = E_K \vec{u}_K(\mathbf{r}), \tag{3}$$

$$\check{H}_{BdG}(\mathbf{r}) = \begin{bmatrix} \hat{H}_0 & \hat{\Delta}(\mathbf{r}) \\ \hat{\Delta}^{\dagger}(\mathbf{r}) & -\hat{H}_0^* \end{bmatrix}, \ \hat{\Delta}(\mathbf{r}) = \Delta(\mathbf{r})i\hat{\sigma}_y. \tag{4}$$

Here, $\vec{u}_K = {}^{\mathrm{t}}(u_{K\uparrow}, u_{K\downarrow}, v_{K\uparrow}, v_{K\downarrow})$ is a four-component vector. The angular momenta are good quantum numbers since the system has rotational symmetry. The eigenvector can be decomposed into angular and radial parts as $\vec{u}_{K=(l,v)}(\mathbf{r}) =$ $\check{U}_l(\theta)\vec{u}_{l,\nu}(r)$ with $\check{U}_l(\theta) = \mathrm{diag}(e^{\mathrm{i}l\theta},e^{\mathrm{i}(l+1)\theta},e^{\mathrm{i}l\theta},e^{\mathrm{i}(l-1)\theta})/\sqrt{2\pi}$ for $\kappa=1$ and $\check{U}_l(\theta) = \mathrm{diag}(e^{\mathrm{i}(l-1)\theta},e^{\mathrm{i}l\theta},e^{\mathrm{i}l\theta},e^{\mathrm{i}(l+1)\theta},e^{\mathrm{i}l\theta})/\sqrt{2\pi}$ for $\kappa = -1$. Here we take ν as the quantum number of radial direction. We can expand this radial part of eigenstate $\vec{u}_{l,v}(r)$ by the Fourier-Bessel expansion⁶⁾ and diagonalize the matrix for each angular momentum l to obtain the set of the eigenvalues and eigenvectors. (Subscripts of the matrix represent the indices of the zeroth points of Bessel functions.) We can find that there are two low energy modes with the energies below the gap in the bulk Δ_b ; One is localized in the vortex core and the other is near the edge. We label them as v = c and v = erespectively. (The definition of Δ_b is mentioned in Sec. 3.) We make a remark on the two zero energy states. In this numerical calculation, we consider the finite-sized but sufficiently large systems, hence two zero energy states have finite but small energies and their signs are opposite. We specify them by v = + and v = -. Each wave function has localized distributions around the vortex core and the edge simultaneously. We can divide them by taking a linear combination of these two states in a proper way and call one of them bound in the vortex core v = c.

We calculate the scattering rates of the vortex core states within the single mode approximation using only a mode v = c obtained above. We consider there exist weak but many scatterers and treat them within SCBA. The scheme to calculate the scattering rates is given in the following form as

discussed in Ref. 28:

$$\check{G}(\boldsymbol{r}, \boldsymbol{r}'; i\omega_n) = \sum_{l} \frac{\check{\tau}_z \vec{u}_{l,c}(\boldsymbol{r}) (\vec{u}_{l,c}(\boldsymbol{r}'))^{\dagger}}{E_{l,c} - \sigma_l(i\omega_n) - i\omega_n},$$
 (5)

$$\sigma_l(\mathrm{i}\omega_n) = \frac{\Gamma_\mathrm{n}}{2\pi^2 N_\mathrm{n}} \sum_{l'} \frac{M_{l,l'}}{E_{l',c} - \sigma_{l'}(\mathrm{i}\omega_n) - \mathrm{i}\omega_n},\tag{6}$$

$$M_{l,l'} = \int r dr \left| \left(\vec{u}_{l,c}(r) \right)^{\dagger} \check{\tau}_z \vec{u}_{l',c}(r) \right|^2, \tag{7}$$

where $\check{\tau}_z = \operatorname{diag}(1,1,-1,-1)$ and $\vec{u}_{l,c}(r)$ denotes the radial part of $\vec{u}_{l,c}(r)$. Γ_n and N_n are, respectively, the impurity scattering rates and the density of states per spin at Fermi energy ϵ_F in the normal state. ω_n is a Fermion Matsubara frequency and in the following we perform the analytical continuation $i\omega_n \to \omega + i\delta$. The density of states (DoS) can be obtained from the Green's function:

$$N(\omega) = \sum_{l} N_{l}(\omega) = \int d\mathbf{r} \operatorname{Im} \left[\frac{1}{\pi} \operatorname{Tr} \, \check{\tau}_{z} \check{G}(\mathbf{r}, \mathbf{r}; i\omega_{n}) \Big|_{i\omega_{n} \to \omega + i\delta} \right].$$
(8)

We define the impurity scattering rates (denoted as Γ) by two ways: The first definition of Γ is half width at half maximum (HWHM) of the spectrum shown as Γ in Fig. 1 and we use this definition in Sec. 3. The second definition of Γ is the inverse of the DoS multiplied by π ($\Gamma = [\text{Im}G]^{-1}$) shown as Γ' in Fig. 1 and we use this definition in Sec. 4. These definitions are equivalent when the spectrum takes the Lorentzian profile.

3. Numerical calculation

In this section, we show the results of numerical calculations for scattering rates. At first, we explain the parameters used in our calculations. We fix the quasiclassical parameter $k_F \xi = 20$, where k_F and ξ are a Fermi momentum and a coherence length, respectively. In order to set this parameter, we consider the homogeneous system with s-wave pair potential $\Delta(\mathbf{r}) = \Delta_0$ for the moment. In the topological phase, the Fermi momentum k_F and Fermi velocity v_F are well-defined since this two bands model has a single Fermi surface for the uniform system. We set Δ_b as the minimum gap of the oneparticle excitation spectrum around $k = k_F$ and define coherence length as $\xi \equiv v_F/\Delta_b$ with this minimum excitation gap Δ_b . (Note the difference between Δ_0 and Δ_b ; Δ_0 is just an amplitude of s-wave pair potential and Δ_b is the minimum excitation gap. In general, they are not same and approximately satisfy $|\Delta_b/\Delta_0| \simeq |\alpha| k_F/(V_z^2 + \alpha^2 k_F^2)^{1/2}$ as Eq. (34).) We set $\mu = 0$ and Δ_0 as the unit of energy and change the ratio of $m\alpha^2/|V_z|$ under the condition: $V_z^2 > \mu^2 + \Delta_0^2$. We remark again that this system has two inequivalent vortices in terms of the symmetry operation. We can distinguish this inequivalence by the relative sign of slopes of vortex core mode and chiral edge mode: $\partial E_{l,c}/\partial l$ and $\partial E_{l,e}/\partial l$ as shown in Fig. 2. We also find that the signs of Zeeman coupling V_{τ} and vorticity correspond to the signs of slopes of chiral edge mode and vortex core mode, respectively.²⁹⁾ This structure is very similar to the chiral pwave SC if we regard the sign of the slope of the edge mode as

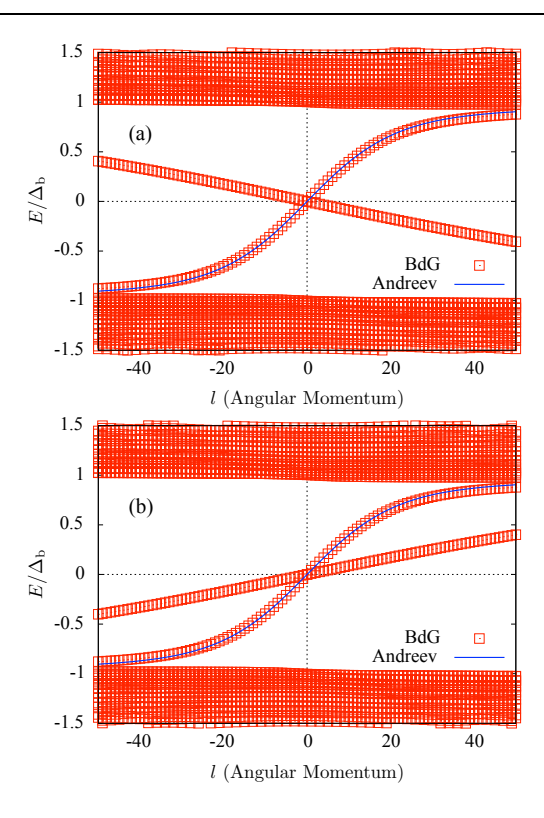
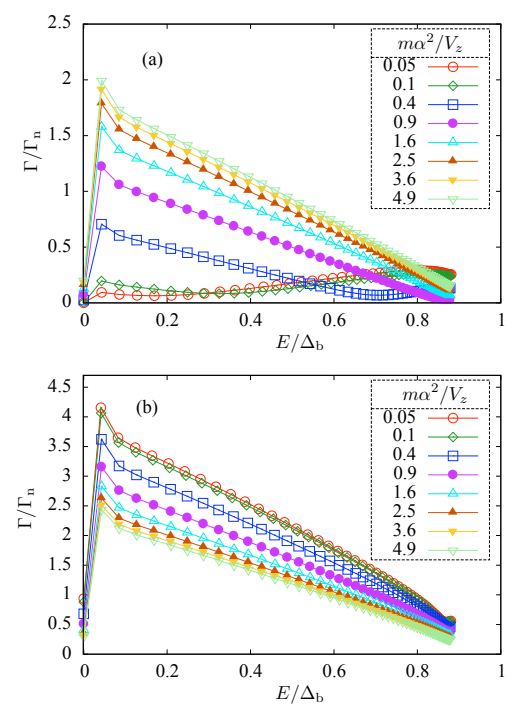


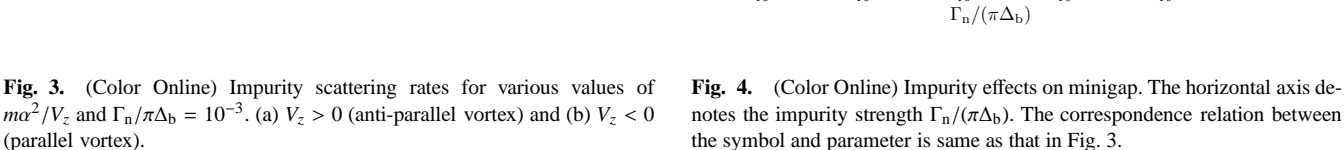
Fig. 2. (Color Online) Energy spectrum for $\mu=0$, $k_{\rm F}\xi=20$, $m\alpha^2/|V_z|=1.6$. (a) The sign of Zeeman coupling is positive and the slopes of two low energy branches are opposite in sign. (b) The sign of Zeeman coupling is negative and the slopes have same sign. The blue-solid line labeled as "Andreev" is the analytical solution for CdGM mode discussed in Sec. 4.

chirality of Cooper pair. We, thus, call the type of vortex with the positive (negative) relative sign "parallel (anti-parallel) vortex". In this system, the signs of the two slopes are same (opposite) when $\kappa V_z > 0$ ($\kappa V_z < 0$) and in the following numerical calculation, we only change the sign of Zeeman coupling and fix the vorticity $\kappa = -1$. To solve the BdG equation, we set the system size $R = 20\xi$ and spatial profile of the pair potential in the radial direction $\Delta(r) = \Delta_0 \tanh(r/\xi)$. Moreover we introduce the two cut-offs: $l_c = 50$ and $N_c = 400$, which are the number of angular momentum as a quantum number and the zero points of Bessel function, respectively, and the infinitesimal quantity $\delta = 10^{-6}\Delta_b$ in Eq. (8). Under these parameters, we numerically solve the BdG equation and Eqs. (5) - (8) to calculate the density of states and scattering rates in the presence of impurities.

We show the scattering rates Γ for various values of $m\alpha^2/|V_z|$ in Figs. 3 (a) and (b), which correspond to the positive and negative Zeeman couplings respectively. The horizontal axis shows the eigen energy for pure systems, which is scaled by the gap Δ_b for each parameter. The discrete eigenenergies scaled by Δ_b are independent of ratio $m\alpha^2/V_z$ and level spacings scaled by Δ_b in low energy are the inverse of $k_F\xi$. We set $\Gamma_n=10^{-3}\pi\Delta_b$. We note again that Δ_b is determined by some parameters such as V_z , $m\alpha^2$ and so on.

(parallel vortex).





10

0.1 0.4 0.9

0.06

0.05

0.04

0.01

0.06

0.05

0.04

0.01

10

10

₫ 0.03 0.02 (a)

(b)

These figures show that the scattering rates for $V_z > 0$ are smaller than those for $V_z < 0$. One might consider that the impurity effects are characterized by the type of vortex (parallel or anti-parallel), because in chiral p-wave SC the bound states in an anti-parallel vortex are robust against impurities, while those in a parallel vortex are sensitive to impurities. Since there are finite scattering rates even for anti-parallel vortex as shown in Fig. 3 (a), it is impossible to characterize the impurity effects only by means of "total angular momentum", which is the sum of the vorticity and chirality of Cooper pairs. We need to consider the dependence on another parameter $m\alpha^2/V_z$. We find that the scattering rates in the low energy region are a decreasing function of the ratio $m\alpha^2/|V_z|$ for the parallel vortex (Fig. 3 (b)), while those are increasing one for the anti-parallel vortex (Fig. 3 (a)). Particularly for very small ratio $m\alpha^2/|V_z| = 0.05, 0.1$, the scattering rates are exceptionally suppressed for the anti-parallel vortex and the difference between the two inequivalent vortices is evident, similarly to the chiral p-wave SC. On the other hand, when $m\alpha^2/|V_z|$ is large, the scattering rates of the two vortices are almost same energy dependence and magnitude, which is a different feature from the case of chiral p-wave SC.

We note again that the adiabaticity of TQC requires the robustness of minigaps and thus we show the Γ_n dependence of the minigap in Fig. 4 (a) for $V_z > 0$ and Fig. 4 (b) for $V_z < 0$. We define the minigap in the presence of impurities by subtracting the widths of first excited state and zero mode from the minigap for pure system as shown in Fig. 1. Impurity effects on minigaps reflect the scattering rates in low energy states. In Fig. 4 (a) only for the case of small $m\alpha^2/|V_z|$ with $V_z > 0$ the minigap is robust against the impurities otherwise, the minigap steeply decreases with increasing Γ_n . In this system the stability of minigap depends on the type of vortices and the parameter $m\alpha^2/V_z$ crucially.

10-1

 $\Gamma_{\rm n}/(\pi\Delta_{\rm b})$

We consider the origin of the dependence on the type of vortices and the parameter within Andreev approximation in next section.

4. Andreev approximation

spectrum and wave functions of low energy states

In this section, we analytically study the bound states in the vortex core within the Andreev approximation for the BdG equation. Tewari and coworkers also discuss the zero energy states in the vortex core by solving the approximated BdG equation analytically.³²⁾ The main strategy of the approximation is same as our following discussion, but the detail of the calculation is slightly different. Moreover our aim is not only the construction of zero energy state but also the construction of non-zero energy states and the understanding of the scattering rates. We also discuss the possibility of construction of the edge state within the Andreev approximation in Appendix

We start with the BdG equation for the uniform case.

$$\check{H}_{BdG}(\mathbf{k})\vec{u}_{\mathbf{k}} = E\vec{u}_{\mathbf{k}} \tag{9}$$

where $\check{H}_{BdG}(k)$ is a 4 by 4 matrix and described as

$$\check{H}_{BdG}(\mathbf{k}) = \begin{pmatrix} \hat{H}_0(\mathbf{k}) & \hat{\Delta} \\ \hat{\Delta}^{\dagger} & -\hat{H}_0^*(-\mathbf{k}) \end{pmatrix}, \qquad (10)$$

$$\hat{H}_{0}(\mathbf{k}) = \begin{pmatrix} \epsilon_{k} + V_{z} & i\alpha k e^{-i\phi_{k}} \\ -i\alpha k e^{i\phi_{k}} & \epsilon_{k} - V_{z} \end{pmatrix}, \ \hat{\Delta} = \begin{pmatrix} 0 & \Delta \\ -\Delta & 0 \end{pmatrix}, \tag{11}$$

$$\epsilon_k = \frac{k^2}{2m} - \mu, \quad \mathbf{k} = k \cos(\phi_k) \mathbf{e}_x + k \sin(\phi_k) \mathbf{e}_y. \tag{12}$$

 \vec{u}_k is a four-component vector and taken as $\vec{u}_k \equiv e^{ik \cdot r} \vec{u}_k$. \vec{u}_k is a spatially oscillating wave function.

First of all, we take the unitary transformation: $\vec{u}_k = \check{U}(k)\vec{u}_k^b = e^{\mathrm{i} k \cdot r} \check{U}(k)\vec{u}_k^b$, in which basis $\hat{H}_0(k)$ is a diagonal matrix. One of the unitary matrices is taken as

$$\check{U}(\mathbf{k}) = \begin{pmatrix} \hat{U}_1(\mathbf{k}) & \hat{0} \\ \hat{0} & \hat{U}_1^*(-\mathbf{k}) \end{pmatrix},$$
(13)

$$\hat{U}_1(\mathbf{k}) = \frac{1}{C} \begin{pmatrix} i\alpha k e^{-i\phi_k} & \sqrt{V_z^2 + \alpha^2 k^2} - V_z \\ \sqrt{V_z^2 + \alpha^2 k^2} - V_z & i\alpha k e^{i\phi_k} \end{pmatrix}, \quad (14)$$

$$C^{2} = 2\sqrt{V_{z}^{2} + \alpha^{2}k_{F}^{2}} \left(\sqrt{V_{z}^{2} + \alpha^{2}k_{F}^{2}} - V_{z}\right). \tag{15}$$

Through this transformation, we obtain the following Hamiltonian:³³⁾

$$\check{H}_{\mathrm{BdG}}^{\mathrm{b}}(\boldsymbol{k})\vec{\bar{u}}_{\boldsymbol{k}}^{\mathrm{b}} = E\vec{\bar{u}}_{\boldsymbol{k}}^{\mathrm{b}}, \quad (16)$$

$$\check{H}_{\mathrm{BdG}}^{\mathrm{b}}(\mathbf{k}) = \check{U}^{\dagger}(\mathbf{k})\check{H}_{\mathrm{BdG}}(\mathbf{k})\check{U}(\mathbf{k}) = \begin{pmatrix} \hat{H}_{0}^{\mathrm{b}} & \hat{\Delta}^{\mathrm{b}} \\ (\hat{\Delta}^{\mathrm{b}})^{\dagger} & -\hat{H}_{0}^{\mathrm{b}} \end{pmatrix}, \quad (17)$$

$$\hat{H}_0^{\text{b}} = \text{diag}(E_{k+}, E_{k-}), E_{k\pm} = \epsilon_k \pm \sqrt{V_z^2 + \alpha^2 k^2},$$
 (18)

$$\hat{\Delta}^{b} = \begin{pmatrix} -if_{p}(k)\Delta e^{i\phi_{k}} & f_{s}(k)\Delta \\ -f_{s}(k)\Delta & if_{p}(k)\Delta e^{-i\phi_{k}} \end{pmatrix}, \quad (19)$$

$$f_s(k) = \frac{V_z}{\sqrt{V_z^2 + \alpha^2 k^2}}, \ f_p(k) = \frac{\alpha k}{\sqrt{V_z^2 + \alpha^2 k^2}}.$$
 (20)

For $V_z^2 > \Delta^2 + \mu^2$, we find $E_{k+} > 0$ and the existence of $k_{\rm F}$ such that $E_{k_{\rm F}-} = 0$. We expand the above BdG eq. (16) around $k_{\rm F}$ with retaining the leading-order terms only, i.e. up to the first-order for E_{k-} and zeroth-order for the other elements. We call this approximation Andreev approximation. We introduce two quantities as follows:

$$E_{k+} \simeq E_{k_{\mathrm{F}}+} = 2\sqrt{V_z^2 + \alpha^2 k_{\mathrm{F}}^2} \equiv E_c, \tag{21}$$

$$E_{k-} \simeq \frac{\partial E_{k-}}{\partial \mathbf{k}} \cdot (\mathbf{k} - \mathbf{k_{\mathrm{F}}})$$

$$= \left(1 - \frac{m\alpha^2}{\sqrt{V_z^2 + \alpha^2 k_F^2}}\right) \frac{\mathbf{k}_F}{m} \cdot (\mathbf{k} - \mathbf{k}_F) \equiv \mathbf{v}_F \cdot (\mathbf{k} - \mathbf{k}_F).$$
(22)

Here the Fermi velocity v_F is parallel to the Fermi momentum k_F . In the following part, we consider a single vortex in the system and set $\Delta = \Delta(r)e^{i\kappa\theta}(\kappa)$: vorticity). We define a 2 by 2 matrix $R(\theta)$ as the rotation around z axis by angle θ and introduce the basis of the 2D polar coordinates as $(e_r, e_\theta) = R(\theta)(e_x, e_y)$. In the bulk region far from the vortex core, $\Delta(r)$ approaches $\Delta_0(>0)$, which is the magnitude of s-wave pairing. Because of this inhomogenity, we replace $(k - k_F)$ by $-i\nabla$ in Eq. (22). In the following, we simply use f_p and f_s instead of $f_p(k_F)$ and $f_s(k_F)$, respectively. We can, thus, write down the differential equation for slowly varying function $\vec{u}_b^{(k)}$ as

$$E_c \bar{u}_{k_{\rm E}+}^{\rm b} - i f_p e^{i\phi_{k_{\rm E}}} \Delta \bar{v}_{k_{\rm E}+}^{\rm b} + f_s \Delta \bar{v}_{k_{\rm E}-}^{\rm b} = E \bar{u}_{k_{\rm E}+}^{\rm b}$$
 (23)

$$-iv_{F} \cdot \nabla \bar{u}_{k_{F^{-}}}^{b} - f_{s} \Delta \bar{v}_{k_{F^{+}}}^{b} + if_{p} e^{-i\phi_{k_{F}}} \Delta \bar{v}_{k_{F^{-}}}^{b} = E \bar{u}_{k_{F^{-}}}^{b}$$
 (24)

$$-E_c \bar{v}_{k_{\rm F}+}^{\rm b} + \mathrm{i} f_p e^{-\mathrm{i} \phi_{k_{\rm F}}} \Delta^* \bar{u}_{k_{\rm F}+}^{\rm b} - f_s \Delta^* \bar{u}_{k_{\rm F}-}^{\rm b} = E \bar{v}_{k_{\rm F}+}^{\rm b} \tag{25}$$

$$\mathrm{i} \nu_F \cdot \nabla \bar{\nu}_{k_{\mathrm{F}^-}}^{\mathrm{b}} + f_s \Delta^* \bar{u}_{k_{\mathrm{F}^+}}^{\mathrm{b}} - \mathrm{i} f_p e^{\mathrm{i} \phi_{k_{\mathrm{F}}}} \Delta^* \bar{u}_{k_{\mathrm{F}^-}}^{\mathrm{b}} = E \bar{\nu}_{k_{\mathrm{F}^-}}^{\mathrm{b}} \tag{26}$$

We can easily eliminate $\bar{u}_{k_{\rm F}^+}^{\rm b}, \bar{v}_{k_{\rm F}^+}^{\rm b}$ and obtain the following two coupled differential equations:

$$\begin{split} \left[-\mathrm{i}\nu_{\mathrm{F}} \cdot \boldsymbol{\nabla} \hat{\sigma}_{z} - \mathrm{Re} \Delta_{p2} \hat{\sigma}_{x} + \mathrm{Im} \Delta_{p2} \hat{\sigma}_{y} \right. \\ \left. + \hat{\Delta}_{s} \hat{A} \hat{\Delta}_{s} \right] \left(\bar{u}_{\mathbf{k}_{\mathrm{F}}^{-}}^{\mathbf{b}} \right) = E \, \hat{\mathbf{1}} \left(\bar{u}_{\mathbf{k}_{\mathrm{F}}^{-}}^{\mathbf{b}} \right), \quad (2) \end{split}$$

where we define $\Delta_{p1,2} = -i f_p e^{\pm i \phi_{k_F}} \Delta$, $\Delta_s = f_s \Delta$ and

$$\hat{A} = \frac{1}{E^2 - E_c^2 - |\Delta_{p1}|^2} \begin{pmatrix} E + E_c & \Delta_{p1} \\ \Delta_{p1}^* & E - E_c \end{pmatrix},$$

$$\hat{\Delta}_s = -i \begin{pmatrix} 0 & \Delta_s \\ -\Delta_s^* & 0 \end{pmatrix}.$$

We can construct the zero energy state (E=0) analogous to the Jackiw-Rebbi solution for massive Dirac equation³⁴⁾ and obtain the low energy spectrum through the first order perturbation even in the presence of \hat{A} . However, the contribution from \hat{A} , i.e. $(\bar{u}_{k_{\rm F}^+}^{\rm b}, \bar{v}_{k_{\rm F}^+}^{\rm b})$, is small compared to that from $(\bar{u}_{k_{\rm F}^-}^{\rm b}, \bar{v}_{k_{\rm F}^-}^{\rm b})$ and we can, thus, omit the forth term in L.H.S. of Eq. (27) and hereafter, analyze the following equation:

$$\left[-i\boldsymbol{v}_{\mathrm{F}}\cdot\boldsymbol{\nabla}\hat{\sigma}_{z}-\mathrm{Re}\Delta_{p2}\hat{\sigma}_{x}+\mathrm{Im}\Delta_{p2}\hat{\sigma}_{y}\right]\begin{pmatrix}\bar{u}_{k_{\mathrm{F}}^{-}}^{b}\\\bar{v}_{k_{\mathrm{F}}^{-}}^{b}\end{pmatrix}=E\hat{1}\begin{pmatrix}\bar{u}_{k_{\mathrm{F}}^{-}}^{b}\\\bar{v}_{k_{\mathrm{F}}^{-}}^{b}\end{pmatrix}.$$
(28)

We take another set of coordinates (s,b) as $(e_s,e_b) = R(\phi_k)(e_x,e_y)$. In this frame, we can find $v_F = v_F e_s$ and take gauge transformation as ${}^{t}(\bar{u}_{k-}^{b},\bar{v}_{k-}^{b}) = \exp[i(\kappa - v_F)]$

 $(1)\phi_{k_{\rm F}}\hat{\sigma}_z/2]^{\rm t}(\tilde{u}_{k_{\rm F}-}^{\rm b},\tilde{v}_{k_{\rm F}-}^{\rm b})$, then Eq. (28) is reduced to

$$\left[-iv_{F}\partial_{s}\hat{\sigma}_{z}-f_{p}\Delta(r)\frac{s}{r}\hat{\sigma}_{y}-\kappa f_{p}\Delta(r)\frac{b}{r}\hat{\sigma}_{x}\right]\begin{pmatrix}\tilde{u}_{k_{F}-}^{b}\\\tilde{v}_{k_{F}-}^{b}\end{pmatrix}=E\hat{1}\begin{pmatrix}\tilde{u}_{k_{F}-}^{b}\\\tilde{v}_{k_{F}-}^{b}\end{pmatrix}.$$
(29)

We note that $r = \sqrt{s^2 + b^2}$ and $\tan(\theta - \phi_{k_F}) = b/s$. b is an impact parameter in scattering theory and related to the angular momentum l through $l = -k_F b$. In this point, we can find that there exists the zero energy state when b = 0. For small b, we treat the third term of Eq. (29) as a perturbation Hamiltonian and obtain other low energy states. We can construct the solution with the energy E = 0 for unperturbed Hamiltonian:

$$\begin{pmatrix} \tilde{u}_{k_{\mathrm{F}^{-}}}^{\mathrm{b}} \end{pmatrix} = \exp\left[-\psi(s,b)\right] \begin{pmatrix} 1 \\ -\mathrm{sgn}(\alpha) \end{pmatrix},\tag{30}$$

$$\psi(s,b) = \frac{1}{v_{\rm F}} \int_0^s ds' \left(\left| f_p \right| \Delta(r') \frac{s'}{r'} \right),\tag{31}$$

where $r' = \sqrt{s'^2 + b^2}$. With this wave function, we can obtain the correction of energy through the first order perturbation:

$$E(b) = \Delta E_1 = \int_0^\infty ds \kappa \left| f_p \right| \Delta(r)(b/r) \exp\left[-2\psi(s, b) \right] / N\xi,$$
(32)

$$N \equiv \int_0^\infty ds \exp\left[-2\psi(s,b)\right]/\xi. \tag{33}$$

The solid lines shown in Fig. 2 represent the energy spectrum given by Eq. (32) for $k_F\xi = 20$ and $m\alpha^2/|V_z| = 1.6$. For this parameter, Eq. (32) is in good agreement with the energy spectrum numerically obtained from BdG equation. For smaller $m\alpha^2/|V_z|$, the deviation of the energy spectrum for large angular momentum is larger, but the low energy spectrum can be described well. From this, the expression of minigap can be approximately obtained:

$$\Delta_{\min} \equiv \left| \frac{1}{k_{\rm F}} \frac{\partial E}{\partial b} \right|_{b=0} = c_1 \frac{|f_p| \Delta_0}{k_{\rm F} \xi} \simeq c_1 \frac{\Delta_b}{k_{\rm F} \xi}, \tag{34}$$

where c_1 is a constant of the order of unity and particularly $c_1 = 7\zeta(3)/\pi^2$ when $\Delta(r) = \Delta_0 \tanh(r/\xi)$.

4.2 scattering rates

Hereafter, making use of the above solutions to the Andreev equation, we calculate the scattering rates for low energy states. In the following calculation, as mentioned in Sec. 2, we change the definition of Γ as the inverse of the DoS multiplied by π ($\Gamma = [\text{Im}G]^{-1}$). We start with Eq. (6). We note that the magnitude of momentum k is k_F within the Andreev approximation. Hence we omit the subscript of ϕ_{k_F} and also use ϕ instead of k_F as a label. We denote $\bar{\phi}$, which satisfies $\bar{\phi} = 2\theta - \phi + \pi$; $\bar{s} = -s$ and $\bar{b} = b$. Without loss of generality, we can take ϕ such that $|\theta - \phi| \le \pi/2$ and in this case $s \ge 0$. In order to use Eq. (6), it is necessary to construct the eigenfunction to the BdG equation approximately. Here we assume that we can approximately describe the eigenfunction by the

following formula:

$$\vec{u}_{l,c}(\boldsymbol{r}) = \frac{e^{\mathrm{i}l\theta}}{\sqrt{2\pi N d\xi r}} \frac{\vec{u}_{\phi}(s,b) + c_2 \vec{u}_{\bar{\phi}}(s,b)}{2},\tag{35}$$

where d is the number of Fermi surface in the normal state and c_2 is a phase factor discussed in Appendix B. We can confirm that this formula is valid for an s-wave SC and a chiral p-wave SC through their analytical expression of BdG wave function (we directly confirm it in Appendix B). We need to obtain \vec{u}_{ϕ} from $\vec{u}_{\phi}^{\text{b}}$ through the unitary and gauge transformations, since \vec{u}_{ϕ} used in Eq. (35) is described in the original basis. Moreover we assume the matrix element $m_{\phi_1,\phi_2} \equiv \vec{u}_{\phi_1}^{\dagger} \, \dot{\tau}_z \vec{u}_{\phi_2}$ satisfies the relation $m_{\phi_1,\phi_2} = -m_{\phi_2,\phi_1}$. This relation is satisfied in the present system, s-wave SC and chiral p-wave SC. Under these assumptions, we evaluate the diagonal elements of Eq. (7):

$$M_{l,l} = \int r dr |2\pi \vec{u}_{l,c}^{\dagger}(\mathbf{r}) \check{\tau}_{z} \vec{u}_{l,c}(\mathbf{r})|^{2}$$

$$= \int \frac{dr}{r} \frac{\left| m_{\phi,\phi} + m_{\bar{\phi},\bar{\phi}} + \left(c_{2} m_{\phi,\bar{\phi}} e^{-2ik_{F}s} + c_{2}^{*} m_{\bar{\phi},\phi} e^{2ik_{F}s} \right) \right|^{2}}{(4Nd\xi)^{2}}$$

$$= \int \frac{dr}{r} \frac{\left| m_{\phi,\bar{\phi}} \right|^{2} \left[1 - \cos(4k_{F}s - 2\beta) \right]}{8(Nd\xi)^{2}}.$$
 (36)

In the last line, we put $c_2 = e^{i\beta}$ and when $k_F\xi$ is large, the integral of the second term is negligible. This expression of the matrix element described by Andreev wave function is general and we also calculate the scattering rates in the case of s-wave SC by the formula in Appendix B. We should evaluate the matrix element $|m_{\phi,\bar{\phi}}|^2$.

$$\left| m_{\phi,\bar{\phi}} \right| = \left[\frac{\sqrt{V_z^2 + \alpha^2 k_F^2} - V_z}{\sqrt{V_z^2 + \alpha^2 k_F^2}} \delta_{\kappa,-1} + \frac{\sqrt{V_z^2 + \alpha^2 k_F^2} + V_z}{\sqrt{V_z^2 + \alpha^2 k_F^2}} \delta_{\kappa,1} \right] \times \left| \sin(\phi - \bar{\phi}) \right| \exp\left[-2\psi(s,b) \right].$$
(37)

This expression shows that impurity effects are same under changing the sign of V_z and κ simultaneously. The difference between parallel and anti-parallel vortices is described only by coefficients $[(V_z^2 + \alpha^2 k_F^2)^{1/2} \pm |V_z|]/(V_z^2 + \alpha^2 k_F^2)^{1/2}$ (+(-): parallel (anti-parallel)). In order to evaluate the integral, we use

$$|\sin(\phi - \bar{\phi})| = 2|\sin(\theta - \phi)\cos(\theta - \phi)| = \frac{2|sb|}{s^2 + h^2},$$
 (38)

and perform the following approximation on the region of integral. The integral in Eq. (36) can be evaluated as

$$\int_{b}^{\infty} \frac{dr}{r} \sin^{2}(\phi - \bar{\phi})e^{-4\psi(s,b)} \simeq \int_{b}^{\xi} \frac{dr}{r} \frac{4s^{2}b^{2}}{(s^{2} + b^{2})^{4}}$$

$$= 1 - \frac{2b^{2}}{\xi^{2}} + \frac{b^{4}}{\xi^{4}}.$$
 (39)

If we focus on the first excited state with angular momentum |l| = 1, we can estimate $b^2/\xi^2 = 1/(k_F\xi)^2$ and omit the second and third terms in Eq. (39). We, thus, obtain the matrix

element $M_{l,l}$ as

$$M_{l,l} = \frac{1}{8(Nd\xi)^2} \left[1 + \frac{\text{sgn}(\kappa V_z) |V_z|}{\sqrt{V_z^2 + \alpha^2 k_F^2}} \right]^2.$$
 (40)

We consider the two limiting cases of the scattering rates in detail. One is that there is large level spacing in the presence of impurities and hence we can neglect the contribution from other angular momentum states. The other is the limit of continuous spectra but the impurity strength is very small and thus we can treat it within non-SCBA.

In the former case, we neglect the contribution to σ_l from other angular momentum states l' in Eq. (6), hence,

$$\sigma_l(i\omega_n) = \frac{\Gamma_n}{2\pi^2 N_n} \frac{M_{l,l}}{E_{l,c} - \sigma_l(i\omega_n) - i\omega_n},\tag{41}$$

$$\sigma_l(E_{l,c}) = i \sqrt{\frac{\Gamma_n}{2\pi^2 N_n} M_{l,l}}, \tag{42}$$

 $\Gamma \equiv \text{Im}\sigma_l(E_{l,c})$

$$= \Gamma_{\rm n} \sqrt{\frac{\pi \Delta_{\rm b}}{8(\pi N d)^2 \Gamma_{\rm n} k_{\rm F} \xi} \left(1 + \frac{\text{sgn}(\kappa V_z) |V_z|}{\sqrt{V_z^2 + \alpha^2 k_{\rm F}^2}}\right)^2}. \tag{43}$$

In the second line, we perform the analytical continuation $\mathrm{i}\omega_n \to \omega + \mathrm{i}\delta$ and set $\omega = E_{l,c}$. We also use $N_\mathrm{n} = k_\mathrm{F}/(2\pi v_\mathrm{F})$ in the last line.

In the latter case, we replace the summation with respect to l' by integration with respect to b' through the relation $l' = -k_F b'$. We focus on the low energy states and thus use the approximate form of energy spectrum: $E_{l',c} = E(b') \simeq \kappa \Delta_{\min} k_F b'$ and put $\sigma_{l'}(i\omega_n) = 0$ in the denominator in Eq. (6), and then we can calculate Γ as follows:

$$\Gamma \equiv \operatorname{Im}\sigma_{l}(E(b)) = \frac{k_{\mathrm{F}}\Gamma_{\mathrm{n}}}{2\pi^{2}N_{\mathrm{n}}} \int db' \operatorname{Im} \frac{M_{l(b)l(b')}}{E(b') - E(b) - \mathrm{i}\delta}$$

$$= \frac{\Gamma_{\mathrm{n}}M_{l,l}}{2\pi N_{\mathrm{n}}\Delta_{\mathrm{mini}}} = \frac{\Gamma_{\mathrm{n}}}{8c_{1}(Nd)^{2}} \left(1 + \frac{\operatorname{sgn}(\kappa V_{z})|V_{z}|}{\sqrt{V_{z}^{2} + \alpha^{2}k_{\mathrm{F}}^{2}}}\right)^{2}. \tag{44}$$

We compare the above two formulas with the numerical calculation. We again make a remark on the definition of scattering rates. In this section, contrarily to the previous section, we define Γ as the inverse of ImG at the energy $E_{l,c}$. In Figs. 5 (a) and (b), we show the scattering rates for the first excited state with angular momentum l=1. The solid lines shown in Figs. 5 (a) and (b) represent the scattering rates by Eq. (43) while dotted lines shown in Fig. 5 (b) those calculated by Eq. (44). The dashed lines with open square and open circle in Figs. 5 (a) and (b) represent the scattering rates based on the iKK scheme Eqs. (5) - (7) for $V_z > 0$ and $V_z < 0$, respectively. All scheme show that when $V_z > 0$ i.e. antiparallel vortex, the scattering rate is an increasing function of $m\alpha^2/|V_z|$ and when $V_z < 0$ i.e. parallel vortex, the scattering rate is a decreasing function of $m\alpha^2/|V_z|$ mentioned in Sec. 3.

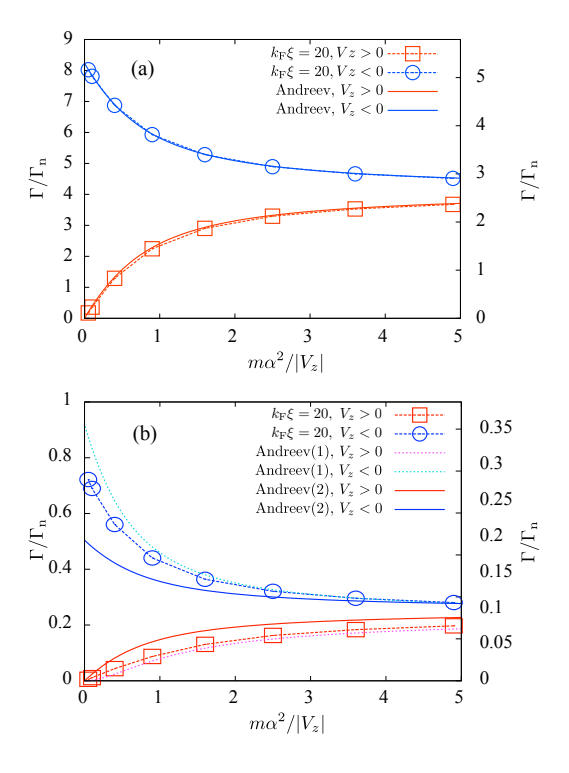


Fig. 5. (Color Online) The scattering rate calculated by means of Andreev approximation (the solid line labeled as "Andreev (1)" corresponds to calculation by Eq. (43) and the dotted line labeled as "Andreev (2)" to that by Eq. (44)) and the scheme Eqs. (5) - (7) (open square for $V_z > 0$ and open circle for $V_z < 0$).

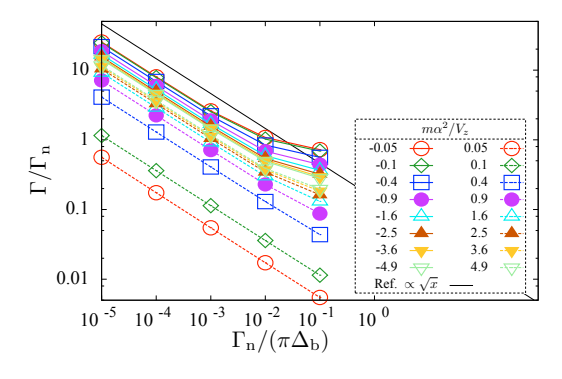


Fig. 6. (Color Online) Γ_n dependence of scattering rates Γ. The solid line denotes the behavior of $[\Gamma_n/(\pi\Delta_b)]^{-1/2}$.

We need to explain vertical axis in Figs. 5 (a) and (b). In Fig. 5 (a), we set $\Gamma_n/(\pi\Delta_b) = 10^{-4}$. The magnitude of the scattering rates based on iKK scheme is shown in the left vertical axis and that based on Eq. (43) is shown in the right vertical axis, which range is 0.64 times smaller than that of the left axis. We tune the range in order to make the parameter dependence clear. In Fig. 5 (b), we set $\Gamma_n/(\pi\Delta_b) = 10^{-1}$ and as well as that in Fig. 5 (a), Γ based on iKK scheme is shown in the left axis

and that based on Eq. (43) is shown in the right axis, which range is 0.33 times smaller than that of the left axis. Moreover, Γ calculated by multiplying Eq. (44) and $\sqrt{2}$ together is also shown in the left axis. (The aim of this operation is just to make the parameter dependence clearer.) The level spacing in this case is $\Delta_{\min}/\Delta_b \sim (k_F \xi)^{-1} = 0.05$ and much larger than $\Gamma/\Delta_b \sim 4\pi \times 10^{-4}$ in Fig. 5 (a). In this case, we can consider that the system is in the limit of discrete spectra and Eq. (43) is valid. On the other hand, in Fig. 5 (b), $\Gamma/\Delta_b \sim 0.2\pi \times 10^{-1}$ and this is comparable to the level spacing. Hence Eq. (43) no longer describes the $m\alpha^2/V_z$ dependence of Γ/Γ_n while this dependence is similar to Eq. (44) except the region of very small $m\alpha^2/|V_z|$ for $V_z > 0$. In this exceptional region, the system has discrete spectra, i.e. the level spacing Δ_{mini} is always larger than the scattering rate Γ since $\Gamma \to 0$ as $m\alpha^2/V_z \to 0$. We infer that Eq. (44) does not explain the dependence precisely even when $V_z < 0$ for the following two reasons. First, we can not regard that the system is in the continuous limit because the scattering rate Γ is not much larger than but comparable to the level spacing Δ_{mini} . Second, we should treat the impurities within SCBA rather than nSCBA, for the impurity strength Γ_{n} is large compared to the level spacing. We emphasize, however, that the $m\alpha^2/|V_z|$ dependence of Γ/Γ_n is similar to Eq. (44) rather than Eq. (43).

Figure 6 shows the $\Gamma_n/(\pi\Delta_b)$ dependence of Γ/Γ_n . We expect $\Gamma/\Gamma_n \propto 1/\sqrt{\Gamma_n/(\pi\Delta_b)}$ from Eq. (43) and Fig. 6 implies that this is a good description for small $\Gamma_n/(\pi\Delta_b)$, approximately for $\Gamma_n/(\pi\Delta_b)$ such that $\Gamma k_F \xi/(\pi\Delta_b) \lesssim 0.1$.

From the above discussions, we find that it is possible to describe impurity effects by Andreev approximation. In the remaining part of this article, we discuss the origin of the scattering rates in terms of the "spin-resolved angular momentum" defined below. As mentioned in the text just below Eq. (4) in Sec. 2, each component of the quasiparticle state labeled as l has angular momentum $(l-1 \uparrow, l \downarrow, l+1 \uparrow, l \downarrow)$ and $(l \uparrow, l+1 \downarrow, l \uparrow, l-1 \downarrow)$ in the original basis when $\kappa = -1$ and 1, respectively. We can understand the origin of the scattering rates by dividing these four components into two pairs such that $(l\sigma, l\sigma)$ and $(l \pm 1\sigma', l \mp 1\sigma')$. This corresponds to considering the projection $P_{z\uparrow(\downarrow)} = (1 \pm \check{\sigma}_z)/2$ with $\check{\sigma}_z = \operatorname{diag}(1, -1, 1, -1)$. For convenience to specify each pair, we introduce the "spin-resolved angular momentum" such that $L_{z\sigma} = \langle -\check{P}_{z\sigma}\check{\tau}_z i\partial_\theta \check{P}_{z\sigma} \rangle$. In this definition, one of two pairs takes $|L_{z\sigma}| = 2$ and the other takes $|L_{z\sigma}| = 0$. Here we review the calculation of Eq. (37) in terms of $L_{z\sigma}$. We symbolically describe a part of the unitary transformation $\vec{u} \rightarrow \vec{u}^b$ as

$$u_{-}^{b} = \sum_{\sigma} a_{-\sigma} u_{\sigma}, \ v_{-}^{b} = \sum_{\sigma} b_{-\sigma} v_{\sigma}.$$
 (45)

We note that $|a_{-\sigma}| = |b_{-\sigma}|$ and $|a_{-\uparrow}|^2 + |a_{-\downarrow}|^2 = 1$. The matrix element $m_{\phi\bar{\phi}}$ also can be described as

$$|m_{\phi\bar{\phi}}| \propto \left| \sum_{\sigma} |a_{-\sigma}|^2 \sin\left(\frac{L_{z\sigma}}{2}(\phi - \bar{\phi})\right) \right| = |a_{-\bar{\sigma}}|^2 \left| \sin\left(\phi - \bar{\phi}\right) \right|. \tag{46}$$

 $\tilde{\sigma}$ denote the spin component with $|L_{z\tilde{\sigma}}|=2$ while the other spin component with $L_{z\sigma}=0$ does not contribute the scattering rates. We make a remark that $|a_{-\sigma}|(\sigma=\uparrow,\downarrow)$ are the degree of mixing u_{\uparrow} and u_{\downarrow} to make the Fermi surface. Therefore, the scattering rates are determined by the ratio of the contribution from the spin component with $|L_{z\sigma}|=2$ to the Fermi surface.

5. Summary

In this paper, we have investigated the impurity effects on the bound (CdGM) states in a vortex core of topological swave SC. We have calculated the scattering rates for CdGM states numerically and analytically. The numerical calculation is performed for discrete spectra based on iKK scheme in order to discuss the impurity effects on the level spacing of bound states. We have found that there are similarity and difference compared to the chiral p-wave SC: the parameter $m\alpha^2/V_7$ is important to describe the impurity effects as well as the relative sign of the vorticity and "chirality". On the other hand, the analytical calculation is based on Andreev approximation to understand the physical picture of impurity scattering and the origin of the parameter dependent scattering rates. The conclusion is that the scattering rates are determined by the ratio of the spin components with $|L_{z\sigma}| = 2$ composing the Fermi surface.

Although the topological s-wave SC belongs to the same class as the chiral p-wave SC, the properties of excited states are more complicated than those in the chiral p-wave SC. However, the vanishingly small scattering rates because of the coherence factors and rotational symmetry is obtained as well as the case of chiral p-wave SC. The topological s-wave SC is more promising than the chiral p-wave SC such as Sr₂RuO₄ in terms of the robust low energy states in a vortex core in TSC due to the continuous rotational symmetry since this superconductivity is expected to appear in the 2DEG in semiconductor-heterostructure while chiral p-wave superconductivity in Sr₂RuO₄ is affected by C₄ point group symmetry.

Acknowledgements

This work was supported by the Program for Leading Graduate Schools, MEXT, Japan. This work was supported by KAKENHI(23244070) from JSPS.

Appendix A: Edge state

We construct the zero energy edge state, which appears near the edge of TSC, in order to confirm that Andreev approximation can describe the feature of TSC. For simplicity, we consider the one dimensional system: a topological s-wave SC in $x \ge 0$ and vacuum in x < 0. The BdG equation for homogeneous topological s-wave SC in one dimension is as follows:

$$\check{H}(k)\vec{u}_k = E\vec{u}_k, \tag{A-1}$$

$$\check{H}(k) = \epsilon_k \check{\tau}_z + V_z \check{\sigma}_z \check{\tau}_z - \alpha k \check{\sigma}_v \check{\tau}_z - \Delta \check{\sigma}_v \check{\tau}_v, \tag{A-2}$$

where k is the one dimensional momentum. $\check{\sigma}$ and $\check{\tau}$ denote Pauli matrices in spin space and Nambu space, respectively

and they are 4 by 4 matrices. The vector \vec{u}_k has four components, $\vec{u}_k = {}^{\rm t}(u_{k\uparrow}, u_{k\downarrow}, v_{k\uparrow}, v_{k\downarrow})$. In a way similar to Sec. 4, we can write down the Andreev equation by introducing slow spatial variance as an edge at x=0, but in this case we impose the boundary condition where the wave function $\vec{u}=0$. Our goal is to construct the low energy, particularly zero energy wave function by linear combination of the zero energy solutions to the Andreev equation, s.t. the wave function satisfies the boundary condition. The Andreev equation with $k=\pm k_{\rm F}$ can be written as

$$\mp \left[i v_{\rm F} \partial_x \hat{\sigma}_z + f_p \Delta(x) \hat{\sigma}_y \right] \underline{\vec{u}}_{\pm k_{\rm F}-}^b = 0. \tag{A.3}$$

The solutions to these equations are given by

$$\underline{\vec{u}}_{\pm k_{\mathrm{F}^{-}}}^{\mathrm{b}} = \begin{pmatrix} 1 \\ -1 \end{pmatrix} \exp \left[\mathrm{i} k_{\mathrm{F}} x - \frac{1}{\nu_{\mathrm{F}}} \int_{0}^{x} f_{p} \Delta(x') dx' \right]. \tag{A-4}$$

The unitary matrix \check{U}_k defined as $\vec{u}_k = \check{U}_k \vec{u}_k^b$ is given by

$$\check{U}_k = \left[i\alpha k \check{\mathbf{I}} + \left(\sqrt{V_z^2 + \alpha^2 k^2} - V_z \right) \check{\sigma}_x \right] / C, \tag{A.5}$$

where C is defined by Eq. (15). In addition to these solutions with Fermi momenta, we construct the zero energy solutions with $k \sim 0$. In this case, we can write down the Andreev equation as

$$\left[V_z \check{\sigma}_z \check{\tau}_z - \mu \check{\tau}_z + i\alpha \partial_x \check{\sigma}_y \check{\tau}_z - \Delta \check{\sigma}_y \check{\tau}_y\right] \vec{u}_0 = 0. \tag{A-6}$$

This eigenvector can be obtained by considering a matrix:

$$\check{B} = \left[V_z \check{\sigma}_x + i \mu \check{\sigma}_y + \Delta \check{\tau}_x \right] / \alpha. \tag{A.7}$$

We can construct the zero energy solutions with positive eigen values $\lambda_i (i=1,2,\cdots)$ and corresponding eigen vectors \vec{b}_i of \vec{B} . When $V_z^2 > \Delta^2 + \mu^2$, there are two positive eigen values and eigen vectors:

$$\alpha \lambda_1 = \sqrt{V_z^2 - \mu^2} - \Delta, \ \vec{b}_1 = {}^{\rm t} (-b_+, -b_-, b_+, b_-),$$
 (A·8)

$$\alpha \lambda_2 = \sqrt{V_z^2 - \mu^2} - \Delta, \ \vec{b}_2 = {}^{t}(b_+, b_-, b_+, b_-),$$
 (A·9)

$$b_{+} = \sqrt{V_z + \mu}/2|V_z|, \ b_{-} = \sqrt{V_z - \mu}/2|V_z|.$$
 (A·10)

With these set of eigen values and eigen vectors, wave functions can be constructed as

$$\vec{u}_{0\lambda_i} = \vec{b}_i \exp\left[-\int_0^x \lambda_i dx'\right] (i = 1, 2), \tag{A.11}$$

which decay far from the edge at x = 0. We consider the linear combination of these bases to satisfy the boundary condition.

$$\vec{u}(x) = C_{+}\vec{u}_{+k_{\text{F}}} + C_{-}\vec{u}_{-k_{\text{F}}} + C_{1}\vec{u}_{0\lambda_{1}} + C_{2}\vec{u}_{0\lambda_{2}}. \tag{A.12}$$

Here we omit the contribution from $\underline{\vec{u}}_{\pm k_{\mathrm{F}}+}^{b}$ and perform the unitary transformation $\check{U}_{\pm k_{\mathrm{F}}}$ to obtain $\vec{u}_{\pm k_{\mathrm{F}}}$. Since we can choose C_{+} and C_{-} such that $C_{+}\vec{u}_{+k_{\mathrm{F}}}+C_{-}\vec{u}_{-k_{\mathrm{F}}}$ is parallel to $\vec{u}_{0\lambda_{1}}$ at x=0, we can find that $C_{2}=0$. We emphasize that it is necessary to consider the k=0 components only for the edge state rather than the vortex core state.

Appendix B: Scattering rates for s-wave SC

The BdG wave function for the CdGM states in a vortex core for s-wave or chiral p-wave SC and its asymptotic behavior for large $k_{\rm F}r$ are described as

$$\underline{\vec{u}}_{l,c} = \begin{pmatrix} u_{l,c\uparrow}(r) \\ v_{l,c\downarrow}(r) \end{pmatrix} = \frac{1}{\sqrt{\tilde{N}}} \begin{pmatrix} J_{l-L_z/2}(k_F r) e^{-K(r)} e^{i(l-L_z/2)\theta} \\ -i e^{iL_z\pi/2} J_{l+L_z/2}(k_F r) e^{-K(r)} e^{i(l+L_z/2)\theta} \end{pmatrix} \\
\sim \frac{e^{il\theta-K(r)}}{\sqrt{2\pi \tilde{N}k_F r}} \begin{pmatrix} e^{-i\theta/2} \left[e^{ig_{l-L_z/2}(k_F r)} + e^{-ig_{l-L_z/2}(k_F r)} \right] \\ -i e^{iL_z\pi/2 + i\theta/2} \left[e^{ig_{l+L_z/2}(k_F r)} + e^{-ig_{l+L_z/2}(k_F r)} \right] \end{pmatrix}, \tag{B·1}$$

$$K(r) = \frac{1}{v_{\rm F}} \int_0^r \Delta(r') dr', \tag{B-2}$$

$$g_l(x) = x + l^2/(2x) - (2l+1)\pi/4,$$
 (B·3)

where \tilde{N} is a normalization constant. $-L_z$ is a sum of vorticity and chirality and for example, $L_z = \mp 1, \mp 2, 0$ for s-wave SC, chiral p-wave SC with the parallel vortex and that with the anti-parallel vortex, respectively. For convenience, we adopt the minus sign in the definition of L_z . Equation (B·1) is reduced to

$$\begin{pmatrix} u_{l,c\uparrow}(\mathbf{r}) \\ v_{l,c\downarrow}(\mathbf{r}) \end{pmatrix} \sim \frac{c_{3}e^{\mathrm{i}l\theta-K(r)}}{\sqrt{2\pi\tilde{N}k_{\mathrm{F}}r}} \times \begin{pmatrix} e^{-\mathrm{i}\theta/2} \left[e^{\mathrm{i}[g_{1,l}(k_{\mathrm{F}}r)-g_{2,l}(k_{\mathrm{F}}r)]} + \mathrm{i}c_{4}e^{-\mathrm{i}[g_{1,l}(k_{\mathrm{F}}r)-g_{2,l}(k_{\mathrm{F}}r)]} \right] \\ -\mathrm{i}e^{\mathrm{i}\theta/2} \left[e^{\mathrm{i}[g_{1,l}(k_{\mathrm{F}}r)+g_{2,l}(k_{\mathrm{F}}r)]} + \mathrm{i}c_{4}e^{-\mathrm{i}[g_{1,l}(k_{\mathrm{F}}r)+g_{2,l}(k_{\mathrm{F}}r)]} \right] \end{pmatrix}, \quad (B\cdot4)$$

$$g_{l,1}(x) = x + (l^2 + L_z^2/4)/(2x),$$
 (B·5)

$$g_{l,2}(x) = L_z l/(2x),$$
 (B·6)

$$c_3 = e^{-i(2l - L_z + 1)\pi/4},$$
 (B·7)

$$c_4 = e^{i(2l - L_z)\pi/2}. ag{B.8}$$

 c_3 is just an overall phase factor and we need not take care of this. We take an approximation that $g_{l,1}(k_F r) \sim k_F |s|$. Of course this approximation is not good in the region where $k_F |s|$ is not large compared to $|l| = k_F |b|$, but we expect that the physical picture does not change so much.

On the other hand, Andreev wave function is described as

$$\begin{pmatrix} u_{\phi} \\ v_{\phi} \end{pmatrix} = \begin{pmatrix} e^{-iL_{c}\phi/2} \\ e^{iL_{c}\phi/2} \end{pmatrix} \exp[ik_{F}s - \psi(s,b)],$$
 (B·9)

$$\psi(s,b) = \frac{1}{v_{\rm F}} \int_0^s \Delta(r') \frac{s'}{r'} ds'. \tag{B.10}$$

As mentioned in the main text, we take ϕ such that $|\theta - \phi| < \pi/2$ hence $s \ge 0$. We consider a linear combination of two momenta ϕ and $\bar{\phi}$, which share the impact parameter b.

$$\begin{split} e^{\psi(s,b)} [\vec{\underline{u}}_{\phi} + c_2 \vec{\underline{u}}_{\bar{\phi}}] \\ &\simeq \begin{pmatrix} [e^{ik_F s + iL_z b/(2r)} + c_2 e^{-iL_z \pi/2} e^{-ik_F s - iL_z b/(2r)}] e^{-iL_z \theta/2} \\ -i[e^{ik_F - iL_z b/(2r)} + c_2 e^{iL_z \pi/2} e^{-ik_F s + iL_z b/(2r)}] e^{iL_z \theta/2} \end{pmatrix} \end{split}$$

$$= \begin{pmatrix} [e^{\mathrm{i}k_{\mathrm{F}}s - \mathrm{i}L_{z}l/(2k_{\mathrm{F}}r)} + c_{2}e^{-\mathrm{i}L_{z}\pi/2}e^{-\mathrm{i}k_{\mathrm{F}}s + \mathrm{i}L_{z}l/(2k_{\mathrm{F}}r)}]e^{-\mathrm{i}L_{z}\theta/2} \\ -\mathrm{i}[e^{\mathrm{i}k_{\mathrm{F}}s + \mathrm{i}L_{z}l/(2k_{\mathrm{F}}r)} + c_{2}e^{\mathrm{i}L_{z}\pi/2}e^{-\mathrm{i}k_{\mathrm{F}}s - \mathrm{i}L_{z}l/(2k_{\mathrm{F}}r)}]e^{\mathrm{i}L_{z}\theta/2} \end{pmatrix}, \tag{B·11}$$

where we use $\theta - \phi \simeq \sin(\theta - \phi) = b/r$ in the second line and $l = -k_{\rm F}b$ in the third line. When *b* is small compared to *s*, $K(r) \sim \psi(s,b)$ and thus we obtain

$$c_2 = ic_4 = e^{i(l+1/2)\pi},$$
 (B·12)

$$\underline{\vec{u}}_{l,c} = \frac{e^{\mathrm{i}l\theta}}{\sqrt{2\pi\tilde{N}k_{\mathrm{E}}r}} \left[\underline{\vec{u}}_{\phi} + c_2\underline{\vec{u}}_{\bar{\phi}} \right]. \tag{B.13}$$

We can choose the normalization constant $\tilde{N} = 4N\xi d/k_F$, where N is defined by Eq. (33) and d is the number of Fermi surface; in this case d = 1. Eq. (35), thus, can be obtained in the case of s-wave and chiral p-wave SCs.

In the remaining part of this appendix, using Eqs. (36) and (44), we calculate the scattering rates of CdGM state in a vortex core in an s-wave SC. In this case, l is a half-odd-integer and $L_z = \pm 1$. We evaluate the matrix element $M_{l,l}$ by Eq. (36);

$$M_{l,l} = \int \frac{dr}{r} \frac{\left| m_{\phi\bar{\phi}} \right|^2}{8N^2 \xi^2}$$

$$= \int_b^\infty \frac{dr}{r} \frac{\left| 2i \sin \left[L_z(\phi - \bar{\phi})/2 \right] \right|^2}{8N^2 \xi^2} e^{-4\psi(s,b)}$$

$$\simeq \int_0^\xi ds \frac{s}{r^2} \frac{\cos^2(\theta - \phi)}{2N^2 \xi^2}$$

$$= \int_0^\xi ds \frac{s^3}{r^4} \frac{1}{2N^2 \xi^2}$$

$$= -\frac{1}{2N^2 \xi^2} \left\{ \ln|b| + \frac{1}{2} \left[1 - \ln(\xi^2 + b^2) - \frac{b^2}{\xi^2 + b^2} \right] \right\}$$

$$\to -\frac{1}{2N^2 \xi^2} \ln(|b|/\xi) \quad (as b \to 0)$$
(B·14)

Noting that $|E(b)| = \Delta_{\min} k_F |b|$, scattering rate is obtained as

$$\frac{\Gamma}{\Gamma_{\rm n}} = -\frac{1}{4\pi N^2 \xi^2 N_{\rm n} \Delta_{\rm mini}} \ln \left[\frac{E(b)}{\Delta_{\rm mini} k_{\rm F} \xi} \right]$$

$$= -\frac{\pi}{c_1 N^2} \ln \left[\frac{E(b)}{\Delta_{\rm mini} k_{\rm F} \xi} \right], \tag{B-15}$$

where the coefficient is the order of 1. This logarithmic dependence of Γ on E(b) is in good agreement with earlier works

by quasiclassical theory.^{35, 36)} Similarly we can calculate the scattering rates of CdGM states for chiral p-wave vortices.

- 1) D. A. Ivanov: Phys. Rev. Lett. 86 (2001) 268.
- C. Nayak, S. H. Simon, A. Stern, M. Freedman, and S. Das Sarma: Rev. Mod. Phys. 80 (2008) 1083.
- 3) M. Z. Hasan and C. L. Kane: Rev. Mod. Phys. 82 (2010) 3045.
- 4) X.-L. Qi and S.-C. Zhang: Rev. Mod. Phys. 83 (2011) 1057.
- J. Alicea, Y. Oreg, G. Refael, F. von Oppen, and M. P. A. Fisher: Nature Physics 7 (2011) 412.
- 6) L. Mao and C. Zhang: Phys. Rev. B 82 (2010) 174506.
- 7) A. R. Akhmerov: Phys. Rev. B 82 (2010) 020509.
- 8) C. Caroli, P. G. de Gennes, and J. Matricon: Phys. Lett. 9 (1964) 307.
- 9) M. M. Salomaa and G. E. Volovik: Phys. Rev. B 37 (1988) 9298.
- G. Volovik: Journal of Experimental and Theoretical Physics Letters 70 (1999) 609.
- 11) N. Read and D. Green: Phys. Rev. B 61 (2000) 10267.
- 12) A. Altland and M. R. Zirnbauer: Phys. Rev. B 55 (1997) 1142.
- A. P. Schnyder, S. Ryu, A. Furusaki, and A. W. W. Ludwig: Phys. Rev. B 78 (2008) 195125.
- 14) S. Ryu, A. P. Schnyder, A. Furusaki, and A. W. W. Ludwig: New Journal of Physics 12 (2010) 065010.
- 15) Y. Kato: J. Phys. Soc. Jpn. 69 (2000) 3378.
- 16) Y. Kato and N. Hayashi: J. Phys. Soc. Jpn. 71 (2002) 1721.
- Y. Maeno, S. Kittaka, T. Nomura, S. Yonezawa, and K. Ishida: J. Phys. Soc. Jpn. 81 (2012) 011009.
- 18) G. Moore and N. Read: Nuclear Physics B 360 (1991) 362.
- 19) L. Fu and C. L. Kane: Phys. Rev. Lett. 100 (2008) 096407.
- J. D. Sau, R. M. Lutchyn, S. Tewari, and S. Das Sarma: Phys. Rev. Lett. 104 (2010) 040502.
- 21) G. Eilenberger: Z. Phys. 214 (1968) 195.
- 22) A. Larkin and Y. N. Ovchinnikov: Sov. Phys. JETP 28 (1969) 1200.
- A. V. Balatsky, I. Vekhter, and J.-X. Zhu: Rev. Mod. Phys. 78 (2006) 373.
- 24) A. Larkin and Y. Ovchinnikov: Phys. Rev. B 57 (1998) 5457.
- 25) A. Koulakov and A. Larkin: Phys. Rev. B 59 (1999) 12021.
- 26) A. Koulakov and A. Larkin: Phys. Rev. B 60 (1999) 14597.
- 27) N. B. Kopnin and V. E. Kravtsov: JETP Lett. 23 (1976) 578.
- 28) Y. Masaki and Y. Kato: arXiv:1505.02553 (2015).
- L.-H. Wu, Q.-F. Liang, Z. Wang, and X. Hu: Journal of Physics: Conference Series 393 (2012) 012018.
- 30) A. Andreev: JETP 19 (1964) 1228.
- 31) G. Volovik: JETP Lett. 57 (1993) 244.
- S. Tewari, J. D. Sau, and S. D. Sarma: Annals of Physics 325 (2010)
- 33) J. Alicea: Phys. Rev. B 81 (2010) 125318.
- 34) R. Jackiw and C. Rebbi: Phys. Rev. D 13 (1976) 3398.
- 35) N. B. Kopnin: JETP Lett. 60 (1994) 130.
- 36) N. B. Kopnin and A. V. Lopatin: Phys. Rev. B 51 (1995) 15291.